Eur Radiol (2012) 22:476–483
DOI 10.1007/s00330-011-2259-3

UROGENITAL

Evaluation of a robotic technique for transrectal MRI-guided prostate biopsies

Martijn G. Schouten · Joyce G. R. Bomers · Derya Yakar · Henkjan Huisman · Eva Rothgang · Dennis Bosboom · Tom W. J. Scheenen · Sarthak Misra · Jurgen J. Fütterer

Received: 3 March 2011 / Accepted: 8 July 2011 / Published online: 29 September 2011

Abstract
Objectives To evaluate the accuracy and speed of a novel robotic technique as an aid to perform magnetic resonance image (MRI)-guided prostate biopsies on patients with cancer suspicious regions.
Methods A pneumatic controlled MR-compatible manipulator with 5 degrees of freedom was developed in-house to guide biopsies under real-time imaging. From 13 consecutive biopsy procedures, the targeting error, biopsy error and target displacement were calculated to evaluate the accuracy. The time was recorded to evaluate manipulation and procedure time.
Results The robotic and manual techniques demonstrated comparable results regarding mean targeting error (5.7 vs 5.8 mm, respectively) and mean target displacement (6.6 vs 6.0 mm, respectively). The mean biopsy error was larger (6.5 vs 4.4 mm) when using the robotic technique, although not significant. Mean procedure and manipulation time were 76 min and 6 min, respectively using the robotic technique and 61 and 8 min with the manual technique.
Conclusions Although comparable results regarding accuracy and speed were found, the extended technical effort of the robotic technique make the manual technique – currently – more suitable to perform MRI-guided biopsies. Furthermore, this study provided a better insight in displacement of the target during in vivo biopsy procedures.

Keywords Transrectal · Prostate · MR-guided · Biopsy · Robot

M. G. Schouten · J. G. R. Bomers · D. Yakar · H. Huisman · D. Bosboom · T. W. J. Scheenen · J. J. Fütterer
Department of Radiology,
Radboud University Nijmegen Medical Centre,
Nijmegen, Netherlands

E. Rothgang
Pattern Recognition Lab,
Friedrich-Alexander-University of Erlangen-Nuremberg,
Erlangen, Germany

E. Rothgang
Center for Applied Medical Imaging,
Siemens Corporate Research,
Germany and Baltimore (MD), USA

S. Misra
MIRA-Institute of Biomedical Technology and Technical Medicine, University of Twente,
Enschede, Netherlands

M. G. Schouten (✉)
Department of Radiology, University Medical Centre Nijmegen,
P.O. Box 9101, 6500 HB Nijmegen, The Netherlands
e-mail: m.schouten@rad.umcn.nl

Introduction

The detection rate of prostate cancer (PCa) in men with elevated and/or rising prostate specific antigen (PSA) after negative transrectal ultrasound -guided biopsy (TRUS-Bx) sessions is poor. Hambrock et al. found a cancer detection rate of 59%, in men with an elevated PSA and multiple negative TRUS-Bx (≥2) sessions, for magnetic-resonance guided biopsies (MRGBx). This is an improvement when compared to 8 to 12-core TRUS-Bx schemes with a detection rate around 17% (TRUS-Bx≥1) [1–3]. Nevertheless, MRGBx is unpleasant for the patient and time-consuming for the radiologist. For these reasons an in-house pneumatically actuated MR-compatible robot was developed where needle-guide direction can be controlled in real-time inside the controller room [4]. Consequently, the patient remains inside the scanner bore. This may decrease procedure time, enhance patient comfort and improve needle-guide positioning.

Eighty-percent of the tumors with a volume larger than 0.5 cm^3 (diameter=1.0 cm) are likely to be clinically significant [5]. Therefore, it is desirable to have a technique with a biopsy error smaller than 5 mm. Different factors, such as needle-guide positioning, patient and prostate motion, and tissue deformation influence the accuracy of needle positioning [6–8]. Consequently, the needle does not always reach the cancer suspicious region (CSR).

In a phantom study the new robotic technique demonstrated a short manipulation time of 5 min (range 3–8 min) and a high accuracy of 3.0 mm (range 0–5.6 mm) for needle positioning [4]. Yakar et al. demonstrated that it is technical feasible to perform transrectal prostate biopsies using the novel robotic technique (n=10) (Fig. 1) [9]. To evaluate and optimize the biopsy procedure in the future, it is necessary to identify and quantify the cause of the biopsy error. Therefore, the purpose of this study was to evaluate the accuracy and speed of the novel robotic technique as an aid to perform MRGBx on patients with CSRs.

Materials and methods

Patients

This study was approved by the ethics review board and written informed consent was obtained from all patients who were biopsied with the robotic technique. From February to September 2010, 13 consecutive patients with an elevated PSA (>4 ng/mL) and at least one negative TRUS-Bx session were included. Patient were included in the robotic patient population based on their willingness. The manual patient population was matched to the robotic population. Prior to the MRGBx, patients received a 3 T (Magnetom TRIO, Siemens, Germany) multi-parametric MRI examination of the prostate for identification of possible CSRs. T2-weighted (T2-w) images in three orthogonal planes, transversal diffusion weighted images (DWI) and dynamic contrast-enhanced (DCE)-MR images (Table 1) were obtained during and after injection of 15 ml gadopentetate dimeglumine with a power injector (Guerbet, Gorinchem, Netherlands). To evaluate the CSR for clinical significance, the criteria for MRGBx reported by Hambrock et al. were applied [3].

CSRs were determined in consensus by 2 readers with at least 6 years of experience in prostate MR reading. From each CSR the volume (in cc) was determined on the MR images, assuming that the lesions were ellipsoids.

MRGBx

MRGBx were performed within 12 weeks after the diagnostic multi-parametric MR examination. Antibiotic prophylaxis was given with 500 mg ciprofloxacin in the morning and evening for three consecutive days, starting the day before biopsy. A schematic representation of the steps taken to perform a biopsy is illustrated in the flow chart (Fig. 2).

A needle-guide filled with gadolinium-doped water was inserted in the rectum of the patient. Subsequently, the needle-guide was mounted to the robotic or manual device (Step 1). The MR imaging protocol (Step 2) for target selection and to navigate on during the biopsy procedure is shown in Table 1.

Targets were selected (Step 3) on these images based on the CSRs found in the diagnostic MRI examination. Manipulation of the needle-guide was done using either the robotic or manual technique (Step 5). After correct alignment of the needle-guide the insertion depth of the needle was measured on a transversal true-FISP (TRUFI) image (Table 1). The patient was slid out the gantry to

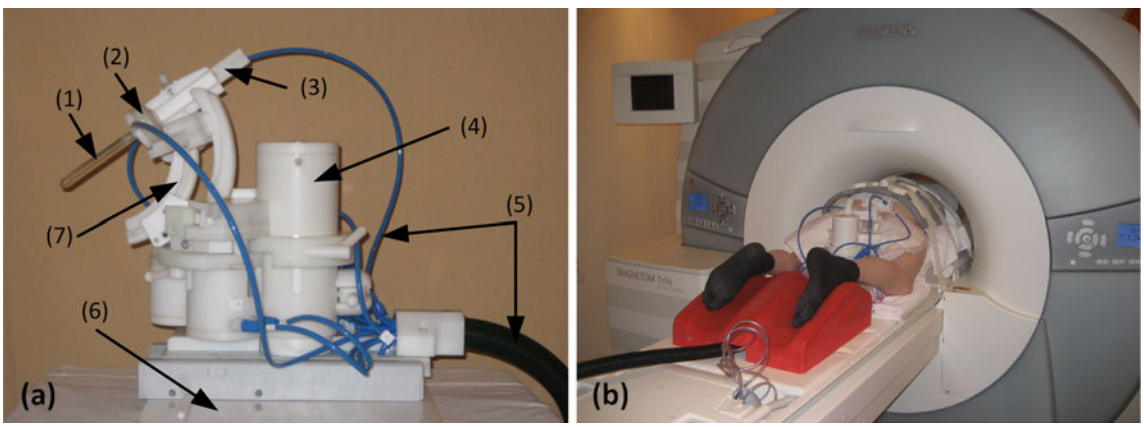

Fig. 1 **a** the robot with (1) the needle guide, (2) safety mechanism with the suction cup, (3) tapping mechanism to introduce the needle guide, (4) pneumatic motor, (5) tubings to the motors, (6) ground plate for installation on the MR table, (7) angulation rail to move the needle guide in the coronal plane. **b** set-up of a patient with the robotic technique on the table of the MR system. The patient was positioned in prone position in the MR system. After the needle guide was inserted rectally it was attached to the robot

Table 1 Imaging protocol with sequence specifications. Volumetric images were utilized to identify anatomical landmarks used to quantify target displacement. * The initial two volumetric images (2/13) were gradient echo sequences (first 2 procedures using the robotic technique)

Sequence	TR/TE/FA ms/ms/ degrees	Resolution (mm)	Acquisition time (minutes)
Diagnostic multi-parametric image sequences			
DWI, b-values: 50, 500, and 800 s/mm^2.	2300–2500/61–64	2.0×2.0×4.0	3:08
Transversal, sagittal and coronal T2-w turbo spin echo	4480–4950/103–110/120	0.6×0.6×3.0	3:22–4:43
DCE-MRI 3D T1-w spoiled gradient-echo	32/1.47/10	1.8×1.8×4.0	2:43
Image sequences during biopsy procedure			
DWI, b-values: 0, 100, 500 and 800 s/mm^2.	2000/67	1.8×1.8×4.0	2:06
T2-w turbo spin echo	3620/103/120	0.8×0.8×4.0	3:26
Transversal and sagittal TRUFI image (manual technique)	4.48/2.24/70	1.1×1.1×3.0	7.5 and 8.9 s
Transversal, sagittal and coronal TRUFI image (robotic technique)	894/2.3/60	1.6×1.6×5.0	0.9 s/slice
T1-w 3D volumetric gradient echo*	4.5/2.2/43	1.0×1.0×1.0	2:20
T2-w 3D volumetric spin echo	1000/102/100	1.0×1.0×1.0	2:36

insert the biopsy needle manually (titanium 18-gauge, fully automatic, core-needle, double-shot biopsy gun with needle length of 175, sampling length of 17 mm (Invivo, Schwerin, Germany).

A T2-w 3D volumetric gradient-echo (first two procedures with the robotic technique) or a T2-w 3D volumetric spin-echo image (all other patients) was acquired with the needle inserted (Step 7). This was the same 3D volumetric image (Table 1) as acquired in step 2. When the needle was in correct position, confirmed on the control images, another target could be targeted (Steps 3–8) or the patient was removed from the MR table (Step 9).

Needle-guide positioning: robotic technique

The robotic system has five degrees of freedom: translations in three directions (anterior-posterior, inferior-superior, lateral) and rotations in two directions (inferior-superior, lateral). The angle of the needle-guide with the main magnetic field could range from 30° to 55° in the inferior-superior direction and plus or minus 26° in the lateral direction [4].

With a simple graphical user interface the direction of the needle-guide can be adjusted [9]. A software package (Interactive Front End (IFE); Siemens Corporate Research, Baltimore (MD), USA) was used to orient and direct the needle-guide in the desired direction (Step 5) under real-time image guidance (Table 1). Manipulation of images and relevant controls can be performed during imaging which allows interactive slice positioning for path planning and real-time monitoring [10, 11].

Needle-guide positioning: manual technique

Transversal and sagittal TRUFI images (Table 1) through the needle-guide were acquired to determine needle-guide direction. The patient was withdrawn from the scanner bore and the radiologist manually adjusted the biopsy device to point the needle-guide towards the

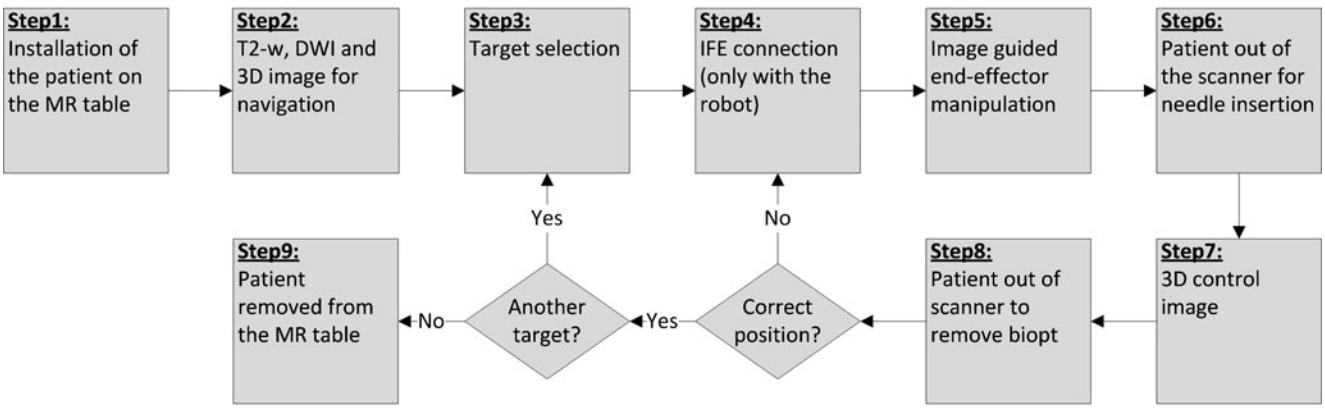

Fig. 2 Flow chart of the biopsy procedure for both the robotic and manual techniques. Scan plane adjustments were only perfomed with the IFE software (step 4) when using the robotic technique

target. To confirm correct positioning of the needle-guide sagittal and transversal TRUFI images were acquired through the needle-guide again. These actions were repeated until the needle-guide was in correct position [12].

Total procedure time and manipulation time were recorded for both the robotic and manual techniques.

Measurements

Motion and deformation of the prostate may occur during the biopsy procedure. This will have effect on the position of the target. Since targeting of the CSR in both methods was done on the images acquired in Step 2, which do not take deformation and motion into account, it is important to distinguish between targeting and biopsy error (Fig. 3).

Targeting error (ε) The targeting error is defined as the normal (shortest) distance from the needle trajectory to the original target location (Fig. 3). This error does not take tissue deformation and patient motion into consideration. This error is a measure for needle-guide positioning towards the intended target.

Biopsy error (δ) The biopsy error is defined as the normal distance from the needle to the transformed target location (the actual target location after needle insertion). The coordinates of the transformed target are corrected for tissue deformation, as well as patient and prostate motion. The transformed target coordinates were calculated by adding the target displacement vector to the original target coordinates.

Target displacement (φ) The target displacement vector is defined by the distance and angle between the original and transformed target location. The target displacement (φ) is the length of this vector. The 3D volumetric images made before (Step 2) and after needle insertion (Step 7) were used to determine the target displacement vector. In these images identical anatomical landmarks around the target (mean 13.7 mm; range 2.3 – 48.4 mm) were manually selected with the aid of an open source fusion package [13]. Calcifications, benign prostate hyperplasia (BPH) nodules, the verumontanum and the urethra were used as anatomical landmarks. Coordinates of these anatomical landmarks (≥5) were used to create a 3D vector field. The arrows represent the direction and distance of displacement of anatomical landmarks (Fig. 4). The mean vector of this vector field is a quantitative measure for localized target displacement, since anatomical landmarks around the target were selected.

To calculate the targeting and biopsy error the needle trajectory was determined by fitting a line through multiple points (≥8) within the needle artifact using linear regression in 3D-space. These points were obtained from the 3D volumetric MR images obtained in Step 7.

Target coordinates (CSRs) were obtained from the T2-w and DW images acquired in Step 2.

The angle between needle trajectory and target displacement direction was calculated in order to see whether the target moved along the needle trajectory or in a random direction (Fig. 5).

Statistical analysis

Two-tailed independent t-tests were performed to determine whether there were significant differences between the robotic and manual techniques for targeting error, biopsy error, target displacement, procedure and manipulation time. Differences were considered to be significant at

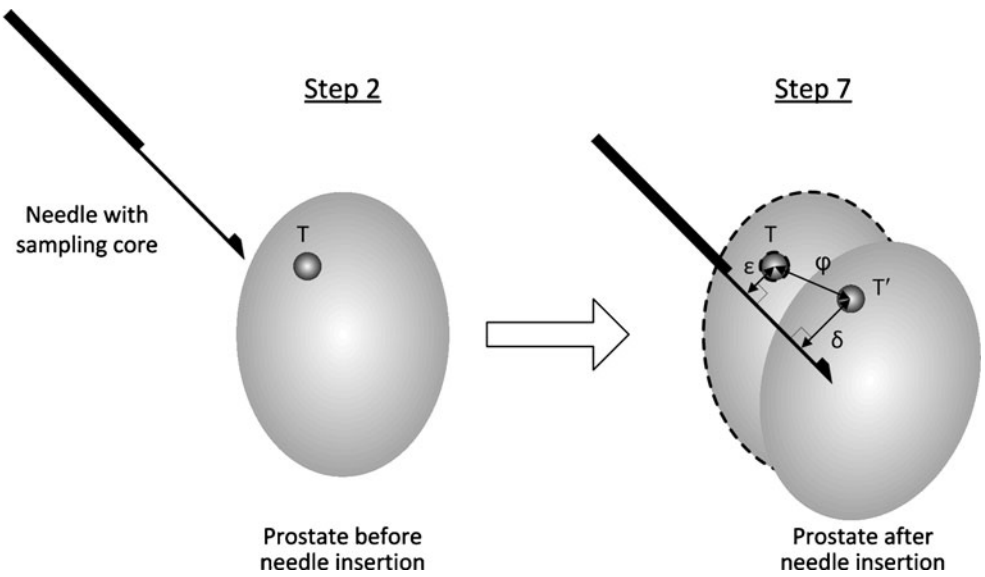

Fig. 3 Representation of the needle inside the prostate, illustrating targeting error (ε), target displacement (φ) and biopsy error (δ). The targeting error, defined as the normal distance from needle to the original target coordinate (T), is shown. Target displacement, defined as the distance between original target (T) and transformed target (T′), is represented by φ. Furthermore, the biopsy error (δ) is shown, which is defined as the normal distance between transformed target (T′) and needle

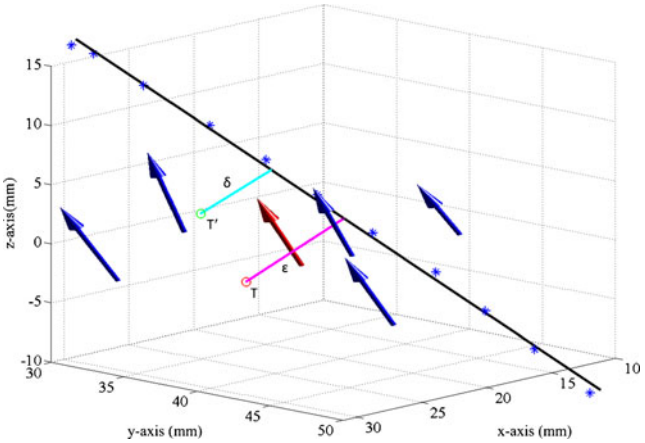

Fig. 4 3D vector field: The blue arrows represent the direction and displacement of the anatomical landmarks. The red arrow is the mean vector representing target displacement. Furthermore, the needle trajectory (black line), targeting error (ε), original target (T), biopsy error (δ) and transformed target (T′) are shown

$p<.05$. Statistical analysis were performed with SPSS, version 16.0.01 (Chicago, Illinois).

Results

In total, 13 patients with 32 needle positions were analyzed. Table 2 describes the patient characteristics and biopsy results for both techniques.

Since the majority of previous negative TRUS-Bx had been performed outside our institution, information on the number of cores was not available for most patients.

Accuracy

The mean targeting error for both the robotic and manual techniques was almost similar (5.7 vs 5.8 mm respectively, $p=0.928$) (Fig. 6). The mean biopsy error was less (4.4 vs 6.5 mm) with the manual technique compared to the robotic technique ($p=0.054$). Target displacement was larger with the robotic technique (6.6 vs 6.0 mm, $p=0.439$).

Direction of target displacement

The mean angle between needle trajectory and target displacement direction for the robotic and manual techniques was 36.7° (range 4.0–82.2°) and 37.6° (range 7.7–73.3°), respectively.

Time

The mean time to perform a biopsy procedure using the robotic technique was 76 min (range 60–100 min) and 61 min (range 52–64 min) with the manual technique. The total procedure time includes the extra time to acquire the 3D volumetric images (2:36 min each). The mean manipulation time to move from target to target was 6 min (range 3–11 min) with the robotic technique and 8 min (range 5–11 min) with the manual technique. The differences in manipulation time and procedure time between both techniques were not significant.

Discussion

The robotic and manual techniques demonstrated comparable results regarding targeting error and target displacement. The biopsy error was larger when using the robotic technique, however not statistically significant. The robotic technique prevented the need of moving the patient in and out of the scanner bore for manipulation and imaging of the needle-guide. Most of the target displacement found in our study was in the direction of the needle trajectory.

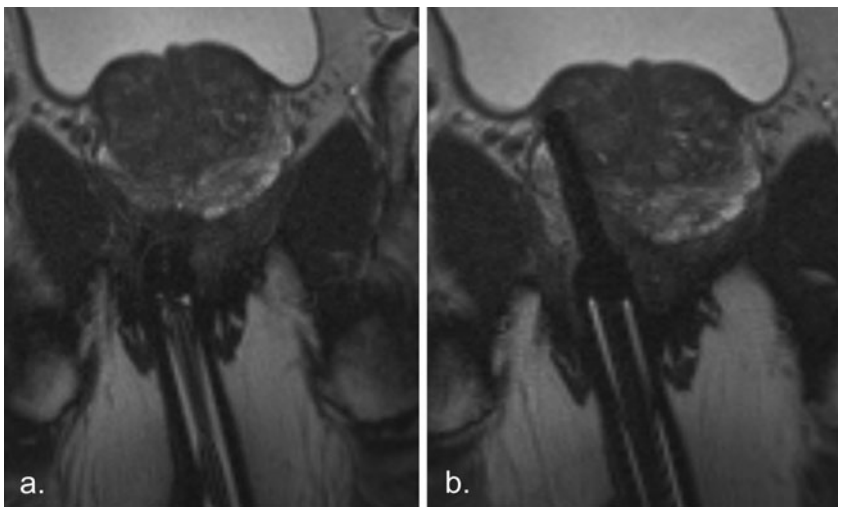

Fig. 5 Transversal TRUFI image through the needle guide before (**a**) and after (**b**) needle insertion in the prostate

Table 2 Patient characteristics and biopsy results for both the robotic and manual techniques

Patient characteristics and biopsy results	Robotic	Manual
Number of patients	8	5
Number of needle placements	19	13
Median needle positions per patient	1.5 (range 1–3)	2 (range 1–4)
Mean PSA (ng/ml)	15 (range 8–28)	14 (range 7–19)
Mean prostate volume (cc)	67 (range 44–98)	72 (range 49–100)
Median number of repeated negative TRUS guided sessions.	2 (range 1–4)	2 (range 1–4)
Median lesion volume on MR images (cc)	0.85 (0.38–1.61)	0.91 (0.6–3.19)
Histopathological findings (nr. of patients)	Non-malignant (3), prostatitis (3), cancer (2)	Non-malignant (2), prostatitis (2), cancer (1)

Several robots for transperineal seed delivery in brachytherapy have been described in literature [14–17]. The robotic and manual techniques for transrectal biopsies demonstrated a larger targeting error (5.7 and 5 mm respectively) compared to other robotic techniques. Muntener et al. found a targeting error of 2.02 mm (range 0.86–3.18 mm) with their robot in a canine model [16]. Zangos et al. describe a transgluteal approach for prostate biopsy with a targeting error of 0.9 mm (range, 0.3–1.6 mm) [18]. The targeting error, biopsy error and target displacement for a transrectal biopsy device were 2.2 mm (range 0.5–5.7 mm), 5.1 mm (range 1.6–11.0 mm) and 5.4 mm (range 1.6–11.1 mm) respectively. Although the targeting error was less compared to our results, the biopsy error and target displacement were in concordance with our results [19].

MR-guided TRUS-Bx may be an alternative to MRGBx in the future because its availability and is probably less expensive. However, initial results show registration errors around three millimeter in phantoms and patients [20–23]. In addition to this error is the targeting error and tissue deformation which together determine the ability to sample a CSR.

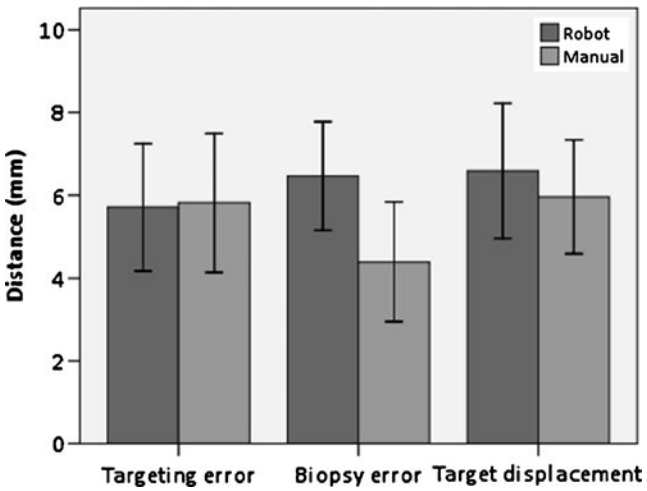

Fig. 6 Histogram showing the mean targeting error, biopsy error and target displacement for both the robotic and manual techniques. The error bars represent the standard deviation

The anatomical landmarks chosen in the MR images to determine target displacement were selected manually. This may have introduced an error, since it is difficult to select exactly the same position. Automatic registration would be an alternative to diminish this error. However, automatic registration is difficult and introduces errors as well [15]. Furthermore, the images that need to be registered are different in the area of the target, because of the presence of the needle, causing a line shape void in the area where best registration is needed.

The biopsy procedures with the robotic and manual techniques were not performed by the same radiologist. To overcome the limitation of inter-variability, the performing physician of each procedure performed the biopsy session in consensus with the first author who attended all sessions.

Despite the fact that patient selection for each technique was not randomly chosen, both groups had similar patient characteristics (Table 2). The number of cores taken during TRUSBx was not available for most patients in both groups.

In the first patient a gradient-echo sequence was used to determine needle trajectory and target displacement. The needle artifact size was acceptable, varying from 3.5 mm to 4.5 mm. In the second patient, the angle of the needle with the static magnetic field was larger. As a result, the artifact size of the needle increased to 8.5 mm. Therefore, we decided to use a 3D spin-echo sequence in which the signal void around the needle was less influenced by distortions of the magnetic field. Needle artifact size now varied from 3.8 to 4.7 mm.

The quantitative method described to determine target displacement cannot discriminate between patient motion, prostate motion and tissue deformation. However, our results demonstrated that most target displacement was in the direction of the needle trajectory suggesting

that most of the target displacement was caused by needle insertion.

Hambrock et al. found a median imaging time of 35 min for MRGBx [24]. In our study, we reported the total procedure times (including patient preparation) for the robotic and manual techniques. Although manipulation time was shorter when using the robotic technique, the total procedure time was longer compared to the manual technique. Positioning of the patient was a precise and time-consuming process. In case of incorrect positioning the whole set-up did not fit inside the scanner bore, or the range of motion of the robotic technique was impaired. Furthermore, a connection with the IFE software was necessary for real-time image guidance. Even for small adjustments in needle-guide direction, a interaction with the IFE was necessary including manual selection of the correct slice direction through the needle-guide. Furthermore, some actions were only possible from behind the MR-console (e.g. measurement tool); the operator had to switch constantly between MR-console and IFE monitor during the procedure. Altogether this led to an extension of the procedure time.

Image registration during the biopsy procedure can correct for target displacement and may attribute to reduce the biopsy error [25]. Nevertheless, image registration is often a time-consuming process. Furthermore, our results suggested that movement of the target was mainly caused by needle insertion. Image registration would not correct for prostate motion due to needle insertion. Deformation models of the prostate to predict tissue deformation due to needle insertion may help to overcome this problem [26]. Other alternatives are different techniques for needle insertion, such as rotating needles and tapping devices [27–30].

Promising treatment types in the MR-scanner such as focal cryosurgery [31] and laser ablation [32] are now under investigation. Major advantages of treatment in the MR scanner are the ability of soft tissue imaging and monitoring (for example temperature mapping) [33]. Robotics will play an important role in the future during treatment in the MR since accurate needle placement is required.

In spite of the fact that the results are comparable regarding accuracy and speed, the larger biopsy error and the extended technical effort of the robotic technique make the manual technique – currently – more suitable to perform MRGBx. Furthermore, this study provided a better insight in displacement of the target during in-vivo biopsy procedures.

Acknowledgement Eva Rothgang received an Educational Grant from Siemens Corporate Research.

References

1. Mian BM, Naya Y, Okihara K et al (2002) Predictors of cancer in repeat extended multisite prostate biopsy in men with previous negative extended multisite biopsy. Urology 60:836–840
2. Roehl KA, Antenor JA, Catalona WJ (2002) Serial biopsy results in prostate cancer screening study. J Urol 167:2435–2439
3. Hambrock T, Somford DM, Hoeks C et al (2010) Magnetic resonance imaging guided prostate biopsy in men with repeat negative biopsies and increased prostate specific antigen. J Urol 183:520–527
4. Schouten MG, Ansems J, Renema WKJ et al (2010) The accuracy and safety aspects of a novel robotic needle guide manipulator to perform transrectal prostate biopsies. Med Phys 37:4744–4750
5. Stamey TA, Freiha FS, McNeal JE et al (1993) Localized prostate cancer. Relationship of tumor volume to clinical significance for treatment of prostate cancer. Cancer 71:933–938
6. Stone NN, Roy J, Hong S et al (2002) Prostate gland motion and deformation caused by needle placement during brachytherapy. Brachytherapy 1:154–160
7. Lagerburg V, Moerland MA, Lagendijk JJ et al (2005) Measurement of prostate rotation during insertion of needles for brachytherapy. Radiother Oncol 77:318–323
8. Damore SJ, Syed AM, Puthawala AA et al (2000) Needle displacement during HDR brachytherapy in the treatment of prostate cancer. Int J Radiat Oncol Biol Phys 46:1205–1211
9. Yakar D, Schouten MG, Bosboom DG et al (2011) Feasibility of a pneumatically actuated mr-compatible robot for transrectal prostate biopsy guidance. Radiology. doi:10.1148/radiol.11101106
10. Lorenz SR, Kirchberg KJ, Zuehlsdorff S et al (2005) Interactive frontend (IFE): a platform for graphical MR scanner control and scan automation. Proc Intl Soc Mag Reson Med 13:2170
11. Yutzy SR, Duerk JL (2008) Pulse sequences and system interfaces for interventional and real-time MRI. J Magn Reson Imaging 27:267–275
12. Beyersdorff D, Winkel A, Hamm B et al (2005) MR imaging-guided prostate biopsy with a closed MR unit at 1.5 T: initial results. Radiology 234:576–581
13. Huisman HJ, Fütterer JJ, van Lin EN et al (2005) Prostate cancer: precision of integrating functional MR imaging with radiation therapy treatment by using fiducial gold markers. Radiology 236:311–317
14. Fischer GS, Iordachita I, Csoma C et al (2008) MRI-compatible pneumatic robot for transperineal prostate needle placement. IEEE/ASME Trans Mechatron 13:295–305
15. Tokuda J, Fischer GS, DiMaio SP et al (2010) Integrated navigation and control software system for MRI-guided robotic prostate interventions. Comput Med Imaging Graph 34:3–8
16. Muntener M, Patriciu A, Petrisor D et al (2008) Transperineal prostate intervention: robot for fully automated MR imaging-system description and proof of principle in a canine model. Radiology 247:543–549
17. van den Bosch MR, Moman MR, van Vulpen VM et al (2010) MRI-guided robotic system for transperineal prostate interventions: proof of principle. Phys Med Biol 55:N133–N140
18. Zangos S, Melzer A, Eichler K (2011) MR-compatible assistance system for biopsy in a high-field-strength system: initial results in patients with suspicious prostate lesions. Radiology 59:903–10
19. Xu H, Lasso A, Vikal S et al (2010) Accuracy validation for MRI-guided robotic prostate biopsy. Medical Imaging 2010: Visualization, Image-Guided Procedures, and Modeling 7625:762517–762518
20. Hu Y, Ahmed HU, Taylor Z et al (2010) MR to ultrasound registration for image-guided prostate interventions. Med Image Anal. doi:10.1016/j.media.2010.11.003

21. Karnik VV, Fenster A, Bax J et al (2010) Assessment of image registration accuracy in three dimensional transrectal iltrasound guided biopsy. Med Phys 37:802–813
22. Martin S, Baumann M, Daanen V et al (2010) MR prio based automatic segmentation of the prostate in TRUS images for MR/TRUS data fusion. Biomedical Imaging: From Nano to Macro, IEEE International Symposium 2010:640–643
23. Singh AK, Kruecker J, Xu S et al (2008) Initial clinical experience with real-time transrectal ultrasonography-magnetic resonance imaging fusion-guided prostate biopsy. BJU Int 101:842–845
24. Hambrock T, Fütterer JJ, Huisman HJ et al (2008) Thirty-two-channel coil 3T magnetic resonance-guided biopsies of prostate tumor suspicious regions identified on multimodality 3T magnetic resonance imaging: technique and feasibility. Invest Radiol 43:686–694
25. Tadayyon H, Lasso A, Gill S et al (2010) Target motion compensation in MRI-Guided prostate biopsy with static images. EMBS Engineering in Medicine and Biology Society (EMBC), Annual International Conference 2010:5416–5419, doi:10.1109
26. Misra S, Macura KJ, Ramesh KT et al (2009) The importance of organ geometry and boundary constraints for planning of medical interventions. Med Eng Phys 31:195–206
27. Abolhassani N, Patel R, Moallem M (2006) Control of soft tissue deformation during robotic needle insertion. Minim Invasive Ther Allied Technol 15:165–176
28. Lagerburg V, Moerland MA, van Vulpen VM et al (2006) A new robotic needle insertion method to minimise attendant prostate motion. Radiother Oncol 80:73–77
29. Lagerburg V, Moerland MA, Konings MK et al (2006) Development of a tapping device: a new needle insertion method for prostate brachytherapy. Phys Med Biol 51:891–902
30. Meltsner MA, Ferrier NJ, Thomadsen BR (2007) Observations on rotating needle insertions using a brachytherapy robot. Phys Med Biol 52:6027–6037
31. Lambert EH, Bolte K, Masson P et al (2007) Focal cryosurgery: encouraging health outcomes for unifocal prostate cancer. Urology 69:1117–1120
32. Lindner U, Lawrentschuk N, Weersink RA et al (2010) Focal laser ablation for prostate cancer followed by radical prostatectomy: validation of focal therapy and imaging accuracy. Eur Urol 57:1111–1114
33. de Senneville BD, Mougenot C, Quesson B et al (2007) MR thermometry for monitoring tumor ablation. Eur Radiol 17:2401–2410